Synchronously Amplified Fluorescence Image Recovery (SAFIRe)

Chris I. Richards, Jung-Cheng Hsiang, and Robert M. Dickson*

School of Chemistry and Biochemistry and Petit Institute for Biosciences and Bioengineering, Georgia Institute of Technology, Atlanta, Georgia 30332-0400

Received: September 23, 2009

Fluorescence intermittency severely limits brightness in both single molecule and bulk fluorescence. Herein, we demonstrate that optical depopulation of organic fluorophore triplet states opens a path to significantly increased sensitivity by simultaneously increasing brightness and greatly reducing background through synchronously detected fluorescence modulation. Image recovery is achieved through selective fluorescence enhancement via modulating a secondary laser excitation at much lower energy than the observed emission in order to depopulate the long-lived triplet states. A series of xanthene dyes that exhibit efficient triplet-state formation demonstrate that this method of selective signal extraction can be achieved at moderate primary and secondary excitation intensities through tailoring dye photophysics and imaging conditions. Up to 5-fold increases in solution-based fluorescence over primary laser excitation alone was achieved upon secondary laser excitation, and dynamic control of signal modulation was demonstrated over a wide time range simply by varying the modulation frequency of the laser used for depopulation of the triplet state. We identify the photophysical characteristics that enable existing or to-be-designed fluorophores to be used in synchronously amplified fluorescence image recovery (SAFIRe) microscopy.

Introduction

Fluorescence microscopy has enabled great advances in both materials science[1,2] and biology,[3−6] yet continued gains in medical imaging and in deciphering low copy protein dynamics in cell biology are fundamentally limited by attainable sensitivity.[7−10] Fluorophore brightness has been engineered to approach fundamental limits for isolated organic dyes, leaving further gains to be achieved through increasing probe size to incorporate degeneracy or by utilizing plasmon-enhanced local excitation.[11,12] Although brighter at low-intensity excitation, these materials come at the cost of size, polyvalency, poor membrane or tissue penetration, and potential toxicity.[7] As brightness often relies on signal visibility on top of background, it is crucial to also reduce both background and noise for true sensitivity increases. Accordingly, researchers have actively pursued creation and optimization of bright fluorophores emitting in the lower background near IR spectral region.[13−15] More active background reduction (or selective signal amplification relative to background) in fluorescence imaging would, however, offer great advantages, but requires optimization of very different photophysical parameters than does brightness alone.

Any process that increases population in the emissive manifold can potentially be used for improving sensitivity. Such processes would transiently produce a higher probability of photon emission, the repeated application of which could then be coupled with lock-in detection for selective signal amplification as is routinely done in high-resolution absorption spectroscopy.[16] Specific modulation of molecular fluorescence is a challenging issue, however, as both background and signal are coupled when modulating the excitation laser.

Normally confounding on the single-molecule level, fluorescence intermittency results in optically induced population of a dark state that causes premature saturation of absorption and limits fluorophore brightness.[17,18] Dark-state traps can arise from varied photoinduced processes such as intersystem crossing,[19] isomerization,[20] or electron transfer.[21] Recently, researchers have utilized dual-laser excitation to capitalize on the disadvantageous traps in thermally stable photoswitches by transient photobleaching, followed by high-energy secondary illumination to regenerate the fluorescent state.[22−25] Such processes in fixed and live cells have enabled both resolution enhancements through sequential single-molecule localization[24−28] and sensitivity increases for selective bulk signal recovery when referenced to an exogenously introduced standard to determine the reference waveform (e.g., OLID, or optical lock-in detection).[22,23] The primary laser in each case is used for both fluorescence excitation and transient photobleaching, while the even higher energy secondary laser recovers the original fluorescent isomer to regenerate the bulk fluorescent signal. Switching times for both processes are intensity dependent and, in OLID, signal recovery is achieved only through cross correlation with signal from an exogenously incorporated reference dye.[22,23] While extremely promising, both sets of methods utilize photoswitches requiring dual high-energy laser excitation, less effectively decoupling detected fluorescence and background.

Complementary to and improving upon OLID, we recently demonstrated that Ag nanoclusters (Ex 633 nm; Em 700 nm) encapsulated in DNA show a dynamic photobrightening on exposure to a lower energy secondary laser (~800 nm) at relatively low intensities.[29] This fluorescence enhancement results from the rapid optical depopulation of a short-lived (~30 μs) dark state. Modulation of this secondary laser results in direct modulation of the higher energy fluorescence in phase with the externally imposed modulation frequency. As most emitters exhibit either no or, at best, exceedingly weak enhancement under extremely high intensity dual-laser excitation,[30] autofluorescence, which typically arises from high concentrations of poor emitters, is also likely to lack the photophysical properties

* To whom correspondence should be addressed. E-mail: dickson@chemistry.gatech.edu.

10.1021/jp909167j
Published on Web 11/10/2009

necessary for efficient optical modulation. Even if some component of the autofluorescent background is weakly modulatable, the nonlinear nature of this excited-state absorption is likely to exhibit a very small modulation depth, especially compared to any SAFIRe-designed fluorophore. Designed emitters could, therefore, significantly improve sensitivity in biological imaging, without need of an exogenous dye photobleaching signal for cross-correlation-based signal extraction. Contrary to that in dual, high-energy laser photoswitching schemes, fluorescence is encoded with the externally applied modulation waveform, enabling direct decoupling from unmodulated background upon demodulation. Dual-laser excitation more rapidly depopulates the dark state, thereby more quickly regenerating the fluorescent manifold and giving a higher probability of emission than with single-laser excitation alone. Fluorescence is specifically recovered from background through Fourier transformation of each pixel vs time to yield the amplitude at the modulation frequency. Unlike fluorescence of interest, background has no increased probability of emission for single vs dual laser illumination and is averaged out over just a few modulation cycles, with the noise decreasing with the square root of the detection time constant used. As detected fluorescence is exactly in phase with the modulation waveform at all incident intensities, simultaneous modulation of the entire field of view coupled with synchronous CCD detection is possible with relatively low excitation intensities. Such synchronously amplified fluorescence image recovery (SAFIRe) enables selective detection at the external modulation frequency to greatly reduce background and noise while amplifying only the signal of interest.

Although only demonstrated to date with novel Ag nanodot fluorophores,[29] such SAFIRe microscopy should be possible with a wide range of organic dyes, if the proper design constraints are considered. For example, fluorescence enhancement of organic dyes due to inefficient reverse intersystem crossing has been reported,[30] but several-fold enhancements were only observed with polymer-immobilized dyes illuminated with extremely high cw secondary-laser intensities ($\sim$MW/cm^2). In solution, most dyes showed only rapid bleaching (i.e., no enhancement), with only a few yielding very modest (10% maximum) enhancement, again under exceedingly high primary ($>5 \times 10^4$ W/cm^2) and secondary laser ($>10^6$ W/cm^2) intensities.[30] Here we demonstrate that through dark state control and use of proper excitation conditions, solution enhancements of even up to 5-fold are readily achieved for various fluorescein derivatives exhibiting significant triplet-state population. Although demonstrated with nonideal dyes to elucidate necessary conditions, similar background reductions with brighter fluorophores should generally enable greatly improved imaging through synchronous detection at moderate excitation intensities.

Theoretical Background

Regardless of origin, the population of dark states limits attainable fluorophore emission rates, particularly at high excitation intensities.[17,31−33] Because transitions to dark states occur with well-defined rate constants and, therefore, quantum yields, high excitation intensities reduce the on-time as more cycles through the emissive state are achieved. Particularly relevant to single-molecule imaging, such fast cycling through the fluorescent state means more dark-state transitions per unit time, leading to increased blinking and premature saturation that limit attainable emission rates. At a given excitation intensity, the total average emission rate prior to true saturation resulting from the inverse of the excitation rate becoming comparable to the excited state lifetime can be modeled as

$$I(\mathrm{avg}) = \frac{\tau_{on}}{\tau_{on} + \tau_{off}} I_{on} + \frac{\tau_{off}}{\tau_{on} + \tau_{off}} I_{off} \qquad (1)$$

in which I_{on} is the burst intensity while cycling within the emissive manifold, I_{off} is the intensity while in the dark state (likely zero, or the background level), τ_{off} is the residence time in the dark state, and τ_{on} is the (excitation-intensity dependent) amount of time before transitioning to the dark state. The longer the residence time in the off state relative to the on-time, the larger the negative effect of premature saturation. Reducing the off-time would then regenerate the linear relation between excitation and emission intensities. Dynamic cycling between saturated (bright) and desaturated (brighter) emissive levels can be achieved by optically depopulating the dark state at regular intervals. A number of factors can greatly affect the complex photophysical interactions, with the most evident being the rate of transition into the dark state (shortens τ_{on}), the stability of the dark state (lengthens τ_{off}), and any modifications of these on- and off-times with excitation intensity.

If optically induced reduction of the off-time occurs at wavelengths longer than that of the collected fluorescence, then the observed increase in emission will be essentially background free, facilitating extremely high sensitivity detection. With this general outline in mind, we selected a series of dyes in the xanthene family: rose bengal, eosin Y, and erythrosin B, all of which have large triplet quantum yields resulting from heavy atom substitution. In analyzing the photophysics of triplet-state depopulation for these dyes, we evaluated the enhancement factor defined as the ratio of emission with dual-laser excitation to that with single-laser illumination under a variety of conditions. The rapid triplet-state depopulation under long-wavelength absorption ensures that the secondary laser generates no additional background fluorescence. Fluorophores were exposed to a primary laser resonant with excitation and a secondary laser sufficiently red-shifted to avoid overlap with the emission. Here we show that significant enhancement can be generated from rose bengal, erythrosin B, and eosin Y in solution, and while these are relatively poor fluorophores for biological imaging, we selected this family of dyes to elucidate conditions under which enhancement is observed, thereby providing information on the design constraints for engineering and selecting fluorophores for SAFIRe microscopy.

Experimental Methods

Rose bengal, erythrosin B, and eosin Y were obtained from Aldrich, and stock solutions were prepared by dissolving the dyes in deionized water (18 MΩ) followed by dilution to experimental concentrations. Samples immobilized in poly(vinyl alcohol) were prepared by diluting the stock solutions of the dye in a saturated solution of PVA and spin coating 100 μL of this solution onto a coverslip at 1000 rpm. All dual-laser experiments were performed on a microscope (Olympus IX 71) using a 60× water-immersion objective (Olympus 1.2 NA) for solution experiments and with a 60× oil-immersion objective (Olympus1.45 NA) for PVA experiments. All solution data was taken by focusing 20 μm into solution. Signals were collected in a confocal arrangement with a multimode fiber serving as the pinhole and directing the emission to a photon counting

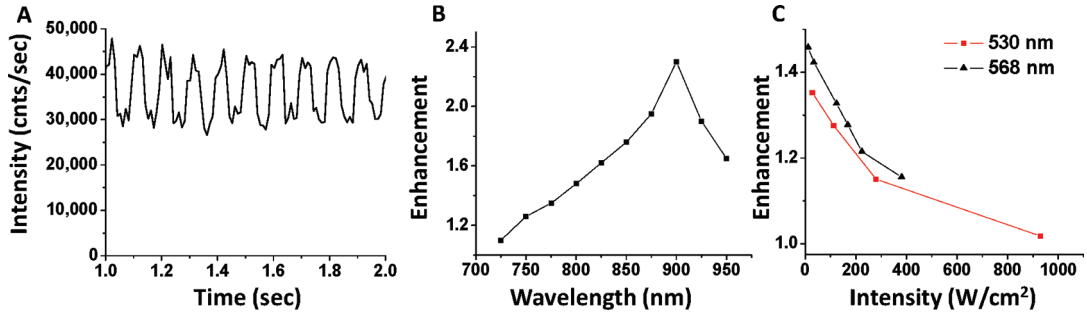

Figure 1. (A) Time trace (binned at 10 ms) of a 10 μM solution of rose bengal excited at 530 nm (50 W/cm^2) with simultaneous excitation at 805 nm (~300 kW/cm^2) modulated at 10 Hz. Clear fluorescence enhancement is observed as arising from secondary laser coillumination. (B) Secondary laser excitation spectrum (350 kW/cm^2 from 725 to 950 nm) with continuous primary excitation at 530 nm (30 W/cm^2). Enhancement is clearly observed beyond 800 nm with a peak near 900 nm. (C) Plot of 530 nm (red) and 568 nm (black) primary intensity vs enhancement factor with constant 805 nm (300 kW/cm^2).

avalanche photodiode (Perkin-Elmer). Intensity trajectories were recorded using a Becker-Hickl photon counting module (SPC 630). Appropriate band-pass filters centered near the emission wavelength of the specific dye were used to efficiently block both the primary excitation and the lower energy secondary laser excitation. Continuous wave primary laser excitation was used near the typical excitation maximum of the dye using a tunable mixed gas (argon/krypton) air-cooled laser (Melles Griot). Experiments involving pulsed primary excitation were performed with a 532 nm pulsed laser (Uniphase) with a repetition rate of 10 kHz. A continuous-wave Ti−sapphire laser (either Coherent Mira or KM Laboratories) was used as the secondary laser excitation source with tunability from 700 to 1000 nm. For experiments utilizing dual-laser excitation, lasers were overlapped using a dichroic mirror prior to entering the microscope and at the sample plane. Modulation of the secondary laser was performed with either a mechanical chopper (Stanford Research Systems) or an electro-optical modulator (ConOptics). A waveform generator (Agilent) triggered and synchronized the modulation devices and detectors. Intensity vs time data was binned at a rate at least 10 times faster than the modulation frequency used. Fourier transformation of the time traces directly reveals the modulation frequency components. Whole-image signal extraction was performed with the dual-laser alignment noted above, and the images were collected with a front-illuminated EM-CCD (Andor) such that the frame rate was 10 times faster than the modulation frequency. Imaging was performed in an epifluorescence setup with a large (defocused) primary laser excitation area and a much smaller focused secondary laser spot. Images were processed by Fourier transformation of each individual pixel intensity vs time to reveal the frequency components. The corresponding amplitude at the modulation frequency of each pixel was used to recover the demodulated image. A more detailed description of SAFIRe-based whole-image demodulation for Ag nanodot fluorescence recovery has been described previously.[29]

Results and Discussion

Rose bengal, erythrosin B, and eosin Y were chosen for their high triplet state quantum yields, while maintaining some fluorescence and having known long-wavelength transient absorptions.[34−36] These dyes and their photophysical trends, coupled with their structural similarities, enable elucidation of the crucial parameters involved in optimizing SAFIRe-compatible dyes. Triplet-state optical depopulation and subsequent repopulation of the singlet manifold has been reported for rose bengal at a variety of wavelengths.[34−36] With these reported parameters in mind, the viability of enhancing the rose bengal emission rate through triplet-state depopulation with dual-laser excitation was explored. Significant enhancement was seen in a 10 μM solution under constant 530 nm excitation with secondary excitation at 805 nm, and was readily modulated by optically chopping the secondary laser beam at 10 Hz (Figure 1A). The fluorescence from primary-laser excitation alone yielded ~30 000 counts/s, while dual-laser excitation yielded ~45 000 counts/s. As emission at higher energy than the secondary laser is collected, the secondary laser introduces no additional background when properly filtered. An enhancement action spectrum was recorded by scanning the secondary-laser wavelength from 725 to 975 nm, with constant primary-laser intensity. Constant intensity at each secondary wavelength was maintained, yielding enhancement as a function of triplet-state depopulation wavelength. The secondary wavelength dependence of enhancement, resulting from back conversion from the triplet state to the emissive state exhibits a peak near 900 nm (Figure 1B). This action cross section (~10^{-18}cm^2)[37] is apparently quite low relative to the triplet absorption cross section (~10^{-16} cm^2) reported from transient absorption studies,[37] presumably due to inefficient back transfer between singlet and triplet manifolds and the high triplet quantum yield once the emissive singlet state is again accessed.

Unfortunately, the rose bengal transient absorption cross section at 532 nm is quite large and on par with that of the singlet to singlet transition.[36] This triplet-state absorption of primary excitation light competes with secondary excitation to independently depopulate the same triplet state, thereby limiting the useful range of primary excitation intensities for rose bengal enhancement (Figure 1C). As transitions to the triplet state are governed by a probability (quantum yield), higher primary-laser excitation intensities lead to shortened on-times as more excitations per second are induced. Rose bengal, however, has a triplet quantum yield exceeding 70% in organic solvents and 98% in aqueous solutions,[35] leading to an average on-time consisting of collecting less than a single photon. Consequently, the effective on-time shortening is negligible as it is already sufficiently limited due to the intrinsically large intersystem crossing rate. Further, the strong triplet state absorption at the primary laser excitation wavelength (530 or 568 nm) makes the enhancement factor decrease significantly with increasing primary laser intensity (Figure 1C). Therefore, rose bengal fluorescence enhancement is only observed at relatively low primary laser intensities (<400 W/cm^2, Figure 1C).

The competing efficient triplet-state absorption at the primary-laser frequency neutralizes expected gains by off-time shorten-

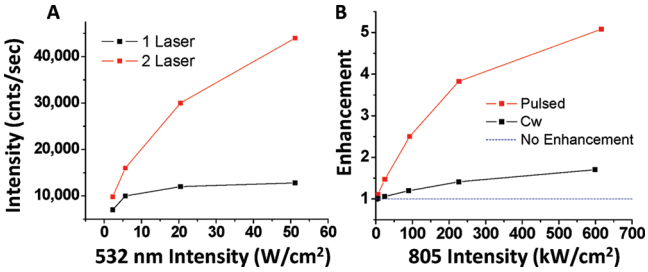

Figure 2. (A) Plot of 532 nm pulsed excitation intensity vs emission rate for single-laser (black) and dual-laser (red) excitation (300 kW/cm^2) comparing the saturation levels showing a substantial increase in the fluorescence. (B) Enhancement factor dependence on the 805 nm secondary-laser intensity for cw (11 W/cm^2) and pulsed (200 W/cm^2) primary excitation.

ing, but suggests that low repetition rate pulsed excitation should yield improved enhancements. Combined with cw secondary illumination, pulsed primary excitation (532 nm, 10 kHz, ~900 ps pulse width) at similar average intensities to those used for continuous wave (cw) excitation further improved enhancement more than 2-fold. As expected, increasing average pulsed primary-excitation intensity yielded increased enhancement factors (Figure 2A). Thus, the long time interval (~100 μs) between subnanosecond primary laser pulses enables the cw secondary laser to independently optically depopulate the triplet state, thereby recovering the expected large fluorescence enhancements (Figure 2B). Resulting from the efficiently populated (98%) and long-lived (~1 ms) triplet level,[35] desaturation of absorption due to low-energy secondary-laser excitation clearly yields significant enhancement of bulk fluorescence by facilitating a larger population in the ground singlet state to be excited with the subsequent 532 nm pulse. Such low-repetition-rate, pulsed primary excitation enables more efficient secondary-laser-induced decay of the triplet state while also allowing higher primary-laser excitation and lower secondary-excitation intensities for brighter overall emission (Figure 2B). Contrary to dual cw excitation, pulsed primary excitation enables maximum enhancement to reach a factor of 5 — by far the largest fluorophore photobrightening observed in solution and with significantly lower intensities than those observed for dyes yielding only 10% maximum enhancement.[30]

While enhancement of rose bengal fluorescence is readily induced, in many ways it is a limiting example based on its very high intersystem crossing rate that restricts the fluorescence quantum yield to only 2%.[35] Consequently, we examined the photophysics of related xanthene dyes, erythrosin Y and eosin b, both differing from rose bengal by varying levels of heavy-atom substitution. All dyes have significant intersystem crossing rates, but both erythrosin and eosin have higher fluorescence quantum yields, with that of eosin exceeding 10%.[38] Similar to published reports demonstrating enhancement with polymer-immobilized eosin, all the dyes presented here readily yielded at least several-fold enhancement when immobilized in polymer films, but at secondary laser intensities (~100 kW/cm^2) an order of magnitude or more lower than those previously reported.[30] Even these lowered photobrightening intensities, however, are still orders of magnitude higher than necessary for enhancement from extremely bright Ag nanodots.[29] These polymer-immobilized enhancements are not shown here as we concentrate on the previously unknown large solution-based enhancements.

Erythrosin B showed very similar characteristics to rose bengal as it was readily enhanced at similar intensities, though as the primary excitation intensity increased above a few hundred W/cm^2, photobleaching rather than enhancement was observed. As previously reported,[30] eosin Y only showed strong primary-laser-induced photobleaching in solution with no enhancement.[30] Given erythrosin B's enhancement and its intermediate intersystem crossing rate and fluorescence quantum yield between those of rose bengal and eosin, we focused additional experiments on eosin in order to further define the optimal conditions for fluorescence enhancement. Analogous to that reported by Ringemann et al.,[30] exposure of an aerated eosin Y solution (1 μM) to simultaneous 530 and 805 nm excitation significantly reduced the fluorescence signal. Removal of oxygen by continuous flow of nitrogen through a sealed fluorescence observation chamber, however, enabled significant fluorescence enhancement to occur on exposure to the secondary laser. Continuous chopping of the secondary laser intensity clearly demonstrates the fluorescence enhancement (Figure 3A) and modulation frequency (1000 Hz) imposed on the fluorescent signal (Figure 3B). The high level of emission corresponds to enhancement and the lower levels to the base single-laser-initiated fluorescence. Primary-laser excitation intensity for eosin Y could reach nearly 1 kW/cm^2 before enhancement dropped from significant competition with secondary 805 nm excitation. This higher primary-laser excitation intensity suggests that the cross section for depopulating the triplet state of eosin Y at 530 nm excitation is significantly lower than that of rose bengal.

A comparison of the three dyes under 532 nm pulsed primary excitation (200 W/cm^2) in deoxygenated aqueous solutions yielded 5-fold rose bengal, 2-fold erythrosin B, and ~10% eosin Y enhancements at identical secondary excitation intensities (Figure 3C). An identical experiment with aerated samples resulted in lower levels of enhancement for both rose bengal (4-fold) and erythrosin B (1.2-fold) presumably from an oxygen-mediated shortening of the triplet state residence. While the large triplet quantum yield for rose bengal (98%) allows for the efficient population of the triplet state even with an individual pulse of the primary laser, the other dyes with lower triplet quantum yields do not so readily transition to the triplet state. The varying enhancement factor between the different dyes reflects the relative triplet quantum yields, with highest to lowest being rose bengal, erythrosin B, and eosin Y. With pulsed excitation the triplet-state population is solely dependent on the quantum yield as long as the pulse power is sufficient to populate the excited state. High action cross sections for both forward and reverse processes are therefore essential for enhancement with low intensity or low duty cycle (pulsed) excitation. The very high intersystem crossing rate of rose bengal, for example enables low primary-laser excitation to yield strong enhancement, but must be coupled with high intensity secondary-laser illumination. Although both eosin Y and erythrosin B have significant triplet quantum yields (56%[34] and 90%,[34] respectively), they are much lower than for rose bengal (98%).[35,39] This enables brighter overall emission but results in lower enhancement levels to be observed.

Directly translatable to dark-state-limited emission rates of much brighter fluorophores (if long-wavelength transient absorptions exist), these fluorophores demonstrate the essential characteristics for background reduction through SAFIRe microscopy. To demonstrate that even moderate levels of enhancement can be used to significantly increase signal visibility, we illuminated a large area with primary excitation (50 W/cm^2) and a subregion with the secondary laser (400 kW/cm^2). Average frames yield rose bengal fluorescence images that simply show a nearly homogeneous fluorescent signal matching that of the primary excitation spot (Figure 4A). Any extra signal resulting

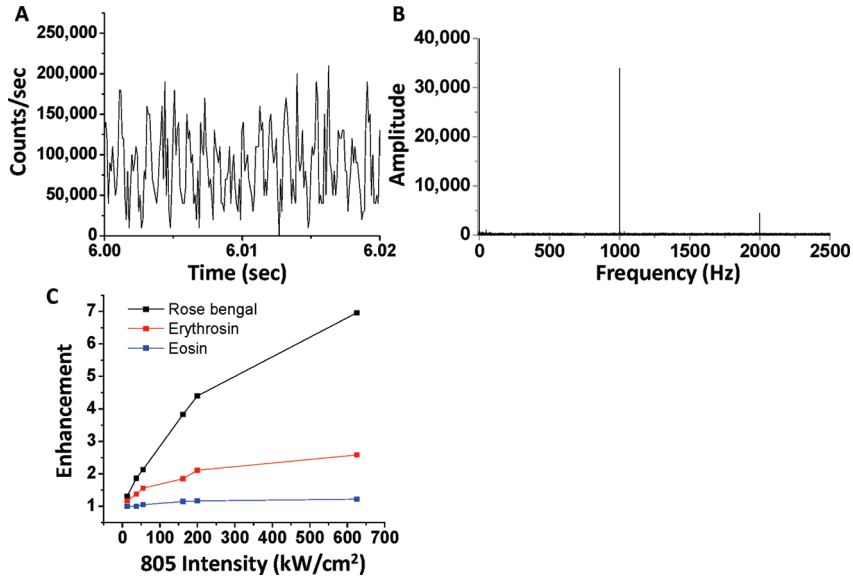

Figure 3. (A) Time trace of deoxygenated, 1 μM aqueous eosin Y with 530 nm (70 W/cm^2) and 805 nm excitation (280 kW/cm^2) modulated at 1000 Hz. Enhancement is in phase with the modulation. (B) Fourier transform of the time trace verifying the frequency component encoded on the fluorescence signal. (C) Enhancement dependence for all three dyes on the 805 nm secondary-laser intensity using 532 nm primary pulsed excitation (200 W/cm^2).

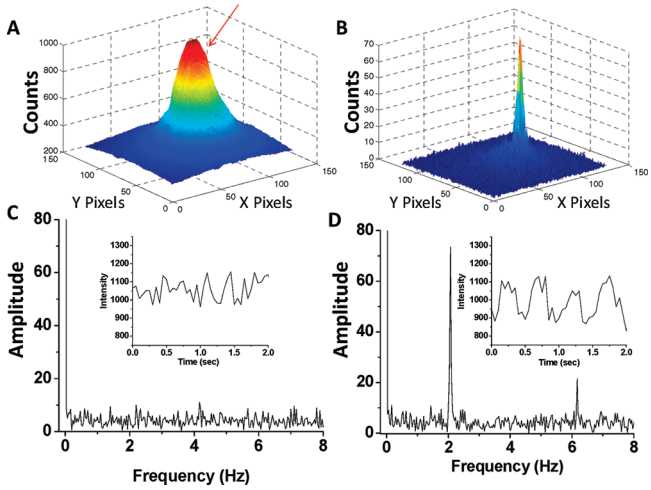

Figure 4. (A) 3-Dimensional plot of the average image of rose bengal solution fluorescence with defocused 530 nm excitation (~50 W/cm^2) and tightly focused 805 nm coexcitation (400 kW/cm^2) modulated at 2 Hz. Synchronous CCD detection was at 20 Hz. The arrow shows the position corresponding to the very small signal increase due to secondary laser excitation. (B) Three-dimensional plot of the demodulated image showing the extraction of the signal from the pixels that are simultaneously exposed to both lasers. (C) Fourier transform of a pixel intensity vs time within an area only exposed to the primary 530 nm laser. The fluorescence trajectory, a representative portion of which is shown as an inset, also shows no modulated component. (D) Fourier transform of a pixel intensity vs time from within an area exposed to both lasers showing the 2 Hz modulation frequency. This modulation frequency component is also seen in a representative portion of the fluorescence trajectory (inset).

from 805 nm secondary illumination is barely distinguishable on top of this background as indicated by the red arrow (Figure 4A). However, the demodulated image recovers only the modulated fluorescence from the much smaller dual-illuminated spot, thereby eliminating essentially all nonmodulated background. The Fourier transforms of the intensity trajectories (Figure 4, insets in parts C and D) of a pixel only exposed to 530 nm laser (Figure 4C) and that from pixels simultaneously exposed to both lasers (Figure 4D) show no modulation frequency component in the single-laser region, but a clear modulation frequency component in the dual-laser-illuminated region, thereby avoiding low-frequency background. Such SAFIRe imaging significantly improves signal visibility and uniquely enables extraction of only the desired signal, with noise decreasing with the square root of the detection time constant. The resulting demodulated image shows a significant reduction in the size of the fluorescent spot such that it matches the size of the original 805-nm laser diameter (Figure 4B), nicely demonstrating that a signal which was buried within high background can be extracted simply by selectively modulating the desired signal. In order to estimate the sensitivity improvement via SAFIRe, the time-averaged image and the demodulated image were compared. In the average image, a typical dual-laser-illuminated pixel (Figure 4, inset in part D) showed a modulated signal amplitude of $A \sim 71$ counts (based on the amplitude of the 2 Hz component in the Fourier transform, Figure 4D). With a background of ~1000 counts, the signal ($2A$) to background ratio is ~0.14. For the demodulated image the modulated signal amplitude, A, is ~71 but now the background has been reduced to ~4 counts, yielding a signal: background of ~18. Thus, as modulation depth is the crucial parameter for signal extraction, even these weakly emitting dyes enable SAFIRe to yield >100-fold improvements in signal visibility. The signal-to-noise improvement can be estimated in a similar fashion. The average counts during dual laser exposure are 1071, while single-laser excitation gives an average count rate of 933, resulting in an enhancement of 138 counts. The noise estimated from the standard deviations of the enhanced and nonenhanced portions of the time trace was 47 and 44, respectively. Subtracting the single-laser-excited background yields an estimated signal (138) to noise ($\sqrt{[44^2 + 47^2]} \sim 64$) of ~2.16. In the demodulated image, only the noise at the modulation frequency (2.1 counts) contributes (as estimated from standard deviation of the frequency dependent intensities in the Fourier transform), yielding a demodulated signal-to-noise of $71/2.1 \sim 34$. This corresponds to a >15-fold signal-to-noise improvement over the averaged, background-subtracted image.

Arising from many potential mechanisms,[19−21] photoexcited dark states are present in all molecules, and usually lead to a

decrease in emission at high, or even moderate excitation intensities. Although immobilization in polymer films enables dual-laser enhancement and potentially modulation, such immobilized systems are largely inapplicable to bioimaging. As with Ag nanodots,[29] our demonstrated ability to dynamically photobrighten (i.e., modulate) emission from various xanthene dyes in solution, however, illustrates general principles for dye modulation leading to selective signal amplification over background, and therefore potentially great utility in SAFIRe microscopy. Despite the fact that the limited brightness of the dyes studied here renders them poor biological imaging agents, they nicely demonstrate the concept of improved sensitivity and lead to a determination of a set of general parameters for engineering and selecting more viable dyes for SAFIRe:

1. Dark-state absorption must be at lower energy than collected fluorescence to avoid generating additional background when modulating.

2. The dark state must naturally decay with some characteristic time.

3. High forward action cross sections (extinction coefficient times dark-state quantum yield) require lower intensity primary illumination.

4. High reverse action cross sections for dark-state depopulation reduce necessary secondary intensities.

5. Maximum enhancement factor is determined by $1 + \tau_{off}/\tau_{on}$, as measured with primary excitation alone.

Conclusion

Owing to their high triplet quantum yields, this series of dyes offers a simple system elucidating the factors yielding optically enhanced and modulated fluorescence. Under the proper experimental conditions, and with relatively low excitation intensities, all three xanthene dyes showed significantly larger enhancements in solution than any previously reported.[30] From the resulting enhancement, photophysical constraints for optimal modulatable dyes were gleaned. The low primary-laser intensities necessary for efficient triplet-state depopulation and the subsequent long-lived nature of the triplet state nicely illustrate that effective dyes for SAFIRe imaging should have moderate quantum yields for dark-state population. While these dyes can be easily modulated and work well for signal extraction experiments, in no way do they represent the ideal fluorophores. Yet, while illustrating the general principles, even these less-than-ideal dyes allow for a significant increase in sensitivity due to modulation and subsequent signal extraction. Giving rise to no additional background and allowing for the extraction of buried signals, the extension of SAFIRe microscopy to more commonly used fluorophores with better photophysical characteristics (i.e., quantum yield and extinction coefficients) that fit the parameters outlined here has the potential to allow for significant advances in biological imaging.

Acknowledgment. R.M.D. gratefully acknowledges financial support from NIH R01-GM068732 and C.I.R. acknowledges NIH NRSA F31EB008324 support.

References and Notes

(1) Wustholz, K. L.; Sluss, D. R. B.; Kahr, B.; Reid, P. J. *Int. Rev. Phys. Chem.* **2008**, *27*, 167–200.
(2) Tata, B. V. R.; Raj, B. *Bull. Mat. Sci.* **1998**, *21*, 263–278.
(3) Liu, S. X.; Bokinsky, G.; Walter, N. G.; Zhuang, X. W. *Proc. Natl. Acad. Sci. U.S.A.* **2007**, *104*, 12634–12639.
(4) Myong, S.; Bruno, M. M.; Pyle, A. M.; Ha, T. *Science* **2007**, *317*, 513–516.
(5) Elf, J.; Li, G. W.; Xie, X. S. *Science* **2007**, *316*, 1191–1194.
(6) Deniz, A. A.; Laurence, T. A.; Beligere, G. S.; Dahan, M.; Martin, A. B.; Chemla, D. S.; Dawson, P. E.; Schultz, P. G.; Weiss, S. *Proc. Natl. Acad. Sci. U.S.A.* **2000**, *97*, 5179–5184.
(7) Taik Lim, Y.; Kim, S.; Nakayama, A.; Stott, N. E.; Bawendi, M. G.; Frangioni, J. V. *Mol. Imaging* **2003**, *2*, 50–64.
(8) Tokunaga, M.; Imamoto, N.; Sakata-Sogawa, K. *Nat. Methods* **2008**, *5*, 455–455.
(9) Sako, Y.; Minoghchi, S.; Yanagida, T. *Nat. Cell Biol.* **2000**, *2*, 168–172.
(10) Kural, C.; Kim, H.; Syed, S.; Goshima, G.; Gelfand, V. I.; Selvin, P. R. *Science* **2005**, *308*, 1469–1472.
(11) Fu, Y.; Lakowicz, J. R. *Laser Photon. Rev.* **2009**, *3*, 221–232.
(12) Nie, S. M.; Emery, S. R. *Science* **1997**, *275*, 1102–1106.
(13) Richards, C. I.; Choi, S.; Hsiang, J. C.; Antoku, Y.; Vosch, T.; Bongiorno, A.; Tzeng, Y. L.; Dickson, R. M. *J. Am. Chem. Soc.* **2008**, *130*, 5038–5039.
(14) Lord, S. J.; Conley, N. R.; Lee, H. L. D.; Nishimura, S. Y.; Pomerantz, A. K.; Willets, K. A.; Lu, Z. K.; Wang, H.; Liu, N.; Samuel, R.; Weber, R.; Semyonov, A.; He, M.; Twieg, R. J.; Moerner, W. E. *ChemPhysChem* **2009**, *10*, 55–65.
(15) Pons, T.; Lequeux, N.; Mahler, B.; Sasnouski, S.; Fragola, A.; Dubertret, B. *Chem. Mater.* **2009**, *21*, 1418–1424.
(16) Bawendi, M. G.; Rehfuss, B. D.; Oka, T. *J. Chem. Phys.* **1990**, *93*, 6200–6209.
(17) Yip, W. T.; Hu, D. H.; Yu, J.; Vanden Bout, D. A.; Barbara, P. F. *J. Phys. Chem. A* **1998**, *102*, 7564–7575.
(18) Garcia-Parajo, M. F.; Segers-Nolten, G. M. J.; Veerman, J. A.; Greve, J.; van Hulst, N. F. *Proc. Natl. Acad. Sci. U.S.A.* **2000**, *97*, 7237–7242.
(19) Yip, W. T.; Hu, D. H.; Yu, J.; Vanden Bout, D. A.; Barbara, P. F. *J. Phys. Chem. A* **1998**, *102*, 7564–7575.
(20) Widengren, J.; Schwille, P. *J. Phys. Chem. A* **2000**, *104*, 6416–6428.
(21) Verberk, R.; van Oijen, A. M.; Orrit, M. *Phys. Rev. B* **2002**, *66*, 4.
(22) Marriott, G.; Mao, S.; Sakata, T.; Ran, J.; Jackson, D. K.; Petchprayoon, C.; Gomez, T. J.; Warp, E.; Tulyathan, O.; Aaron, H. L.; Isacoff, E. Y.; Yan, Y. *Proc. Natl. Acad. Sci. U.S.A.* **2008**, *105*, 17789–17794.
(23) Mao, S.; Benninger, R. K. P.; Yan, Y. L.; Petchprayoon, C.; Jackson, D.; Easley, C. J.; Piston, D. W.; Marriott, G. *Biophys. J.* **2008**, *94*, 4515–4524.
(24) Bates, M.; Huang, B.; Dempsey, G. T.; Zhuang, X. *Science* **2007**, *317*, 1749–1753.
(25) Betzig, E.; Patterson, G. H.; Sougrat, R.; Lindwasser, O. W.; Olenych, S.; Bonifacino, J. S.; Davidson, M. W.; Lippincott-Schwartz, J.; Hess, H. F. *Science* **2006**, *313*, 1642–1645.
(26) Hess, S. T.; Girirajan, T. P. K.; Mason, M. D. *Biophys. J.* **2006**, *91*, 4258–4272.
(27) Hu, D.; Tian, Z.; Wu, W.; Wan, W.; Li, A. D. Q. *J. Am. Chem. Soc.* **2008**, *130*, 15279–15281.
(28) Dedecker, P.; Hotta, J. I.; Flors, C.; Sliwa, M.; Uji-I, H.; Roeffaers, M. B. J.; Ando, R.; Mizuno, H.; Miyawaki, A.; Hofkens, J. *J. Am. Chem. Soc.* **2007**, *129*, 16132–16141.
(29) Richards, C. I.; Hsiang, J.-C.; Senapati, D.; Patel, S.; Yu, J.; Vosch, T.; Dickson, R. M. *J. Am. Chem. Soc.* **2009**, *131*, 4619–4621.
(30) Ringemann, C.; Schonle, A.; Giske, A.; von Middendorff, C.; Hell, S. W.; Eggeling, C. *ChemPhysChem* **2008**, *9*, 612–624.
(31) Yeh, H. C.; Puleo, C. M.; Ho, Y. P.; Bailey, V. J.; Lim, T. C.; Liu, K.; Wang, T. H. *Biophys. J.* **2008**, *95*, 729–737.
(32) Vogelsang, J.; Cordes, T.; Tinnefeld, P. *Photochem. Photobiol. Sci.* **2009**, *8*, 486–496.
(33) Sabanayagam, C. R.; Eid, J. S.; Meller, A. *J. Chem. Phys.* **2005**, *123*.
(34) Gratz, H.; Penzkofer, A. *Chem. Phys.* **2001**, *263*, 471–490.
(35) Larkin, J. M.; Donaldson, W. R.; Knox, R. S.; Foster, T. H. *Photochem. Photobiol.* **2002**, *75*, 221–228.
(36) Reindl, S.; Penzkofer, A. *Chem. Phys.* **1996**, *211*, 431–439.
(37) Larkin, J. M.; Donaldson, W. R.; Foster, T. H.; Knox, R. S. *Chem. Phys.* **1999**, *244*, 319–330.
(38) Reindl, S.; Penzkofer, A. *Chem. Phys.* **1996**, *213*, 429–438.
(39) Stiel, H.; Teuchner, K.; Paul, A.; Leupold, D.; Kochevar, I. E. *J. Photochem. Photobiol. B—Biol.* **1996**, *33*, 245–254.

JP909167J